RSC Advances

PAPER

View Article Online
View Journal | View Issue

Cite this: *RSC Adv.*, 2025, **15**, 46967

The synthesis of PEG/MoS_2-modified biochar for the efficient removal of Cr(VI) in solution: performance and mechanism

Weiyun Yang,[a] Qi Chen[b] and Muqing Qiu *[cd]

Received 18th September 2025
Accepted 12th November 2025

DOI: 10.1039/d5ra07062g

rsc.li/rsc-advances

A highly efficient new type of biological adsorbent (PEG/MoS_2@BC) was prepared *via* hydrothermal synthesis using rice straw biochar, polyethylene glycol, and molybdenum disulfide as raw materials. The effects of different factors on the adsorption performance of PEG/MoS_2@BC for removing Cr(VI) ions from aqueous solutions were analyzed through various experiments. The experimental results indicate that a PEG-MoS_2 composite material was successfully loaded onto the surface of biochar. There was a large number of functional groups on the surface of PEG/MoS_2@BC. Polyethylene glycol and biochar effectively reduced the aggregation of MoS_2. The process for the adsorption of Cr(VI) by PEG/MoS_2@BC can be better described using the pseudo-second-order model and the Langmuir model. The adsorption of Cr(VI) ions was an endothermic chemical process. The reaction mechanism for PEG/MoS_2@BC removing Cr(VI) ions mainly includes complexation reactions, reduction reactions, electronic attraction, and physical adsorption. After five reuse cycles, the adsorption rate still reached 80.23%. The adsorption material PEG/MoS_2@BC exhibited high reusability and stability.

1 Introduction

Chromium (Cr) is a heavy metal with strong solubility, mobility and toxicity, and is widely used in chemical, smelting, electroplating, dyeing and printing industries.[1–5] This can lead to high levels of Cr being released into the environment through wastewater and solid residues. Once discharged into water, Cr can persist. Then, it will bioaccumulate in aquatic organisms and contaminate the food chain. Due to the accumulation of heavy metal pollutants in the food chain, human beings, who sit at the top of the food chain, are the most affected. Bioaccumulation, biomagnification and toxic effects are the main consequences of heavy metal pollution. Water pollution caused by the heavy metal Cr can have an extremely serious influence on the ecological environment and human health. Therefore, we need to explore reasonable methods and technologies to treat Cr-containing wastewater to reduce the negative impact of Cr on the environment and on humans. Hexavalent chromium (Cr(VI)) and trivalent chromium (Cr(III)) are two kinds of Cr compounds found in water. Cr(VI) exhibits superior biological toxicity than Cr(III). Cr(VI) can be teratogenic, carcinogenic, and mutagenic, and can damage the liver and kidneys. It is one of three internationally recognized carcinogenic metals.[6,7] Therefore, Cr(VI) removal is key to controlling Cr pollution in water.

At present, the main treatment methods for heavy metal pollution in water are chemical precipitation,[8] photocatalytic reduction,[9] ion exchange,[10] electrochemical reduction[11] and adsorption reduction.[12] Compared with the adsorption method, other methods are costly and sometimes can cause secondary pollution due to chemical dosing. Adsorption has several advantages as a treatment method for heavy metal removal. It is a simple, cost-effective, and widely applicable technique. It can remove a wide range of heavy metals in both batch and continuous flow systems. Adsorbents can be easily regenerated and reused, reducing waste generation. The basic principle is that Cr(VI) can be adsorbed and removed by some materials with large areas and high porosity that are rich in surface functional groups and have abundant active sites. Therefore, in recent years, the adsorption method for the removal of heavy metal Cr(VI) pollution has made great progress for water remediation. Moreover, adsorption can be combined with other treatment processes, such as filtration or ion exchange, to enhance the overall removal efficiency. In other words, the adsorption method is highly efficient, inexpensive, and uses simple equipment.[13–15] Overall, adsorption is a valuable method for the treatment of water contaminated with heavy metals. It offers a reliable and efficient way to remove heavy metals and protect both the environment and human health.

[a]*Pharmaceutics and Materials Engineering School, Jinhua Polytechnic, Haitang West Street 888, Jinhua, 321007, P. R. China*

[b]*Shaoxing Ecological Environmental Monitoring Center of Zhejiang Province, Shaoxing, 312000, P.R. China*

[c]*College of Life and Environmental Science, Shaoxing University, HuangCheng West Street 508, Shaoxing, 312000, P.R. China. E-mail: qiumuqing@usx.edu.cn*

[d]*Shaoxing Jiangxianghe Agricultural Development Co., Ltd, Shaoxing 312000, PR China*

Widely used adsorbents include silica gel, montmorillonite, and biochar. In recent years, the use of biochar, as a new multifunctional and environmentally friendly material, in environmental remediation research has been increasing. It has become one of the current environmental science research hotspots.[16–21] Biochar is a good adsorption material that has a well-developed pore structure, large specific surface area, many oxygen-containing functional groups, a large cation exchange capacity, and strong adsorption, anti-oxidation, and anti-biodegradation capacities.[22–25] However, in the remediation of heavy metal-polluted water, especially when multiple metals are present, using biochar alone is not very effective. Therefore, to further improve the adsorption capacity of biochar, more and more scholars have begun to study and synthesize a series of new functional biochar composites by various methods of surface modification. This can improve the properties of biochar and its adsorption capacity, and enhance its effect in the remediation of environmental pollution.[26–29] With a high specific surface area and many adsorption sites, molybdenum disulfide (MoS_2) is a graphene-like layered material with Mo atoms sandwiched between two tightly packed layers of hexagonal S atoms.[30,31] In addition, the surface of MoS_2 is rich in sulfide groups with Lewis basicity, especially under acidic conditions. Therefore, these can be used as active sites for selective binding to metals, effectively adsorbing heavy metal ions, including lead, copper, nickel, chromium and so on. As a result of the above advantages, MoS_2 can serve as an effective heavy metal adsorbent, which can be used in the treatment of heavy metal pollution in water. Composite particles of MoS_2 and rice hull carbon (BC/MoS_2) were prepared by a coprecipitation method. Some researches showed that MoS_2 particles could be uniformly distributed on the surface of carbon.[32–34] However, the spacing between S–Mo–S layers in MoS_2 is narrow. Thus, it is difficult for the adsorbate to be adsorbed into the narrow middle layer.[35] Furthermore, MoS_2 has poor dispersion, and the contact area is significantly reduced. Therefore, to make up for its deficiencies and improve its adsorption performance, it is necessary to modify the surface of MoS_2. Polyethylene glycol (PEG) is a non-toxic, eco-friendly, and biocompatible polymer with flexible chains.[36,37] It is made from the polymerization of ethylene glycol. Because of its large number of oxygen, hydroxyl and other active groups, the adsorption capacity of PEG is high. In addition, PEG has high chemical and thermal stability. Therefore, it can maintain stability over a wide range of pH and temperature, and it is not easily damaged by acid, alkali and high-temperature conditions, or other environmental factors. Zhao *et al.* showed that PEG as a MoS_2 surface modifier can improve the dispersion of MoS_2.[38] It was also demonstrated that PEG-modified MoS_2 had good dispersion in water.[39] When the surfactant PEG was introduced, the biocompatibility of the composite was increased and the environmental risk was reduced, while nZVI was effectively loaded onto the BC surface, improving the physical stability of the composite.[38,40–42]

If we use PEG as a surface modifier for MoS_2 and load it onto the surface of biochar, we can achieve the goal of a "win–win effect". This can not only make full use of the advantages of the three materials but can also solve the problem of MoS_2 dispersion for various applications. Thus, this can enhance the stability of MoS_2 when fixed on the surface of biochar and change the physical and chemical properties of biochar. It is beneficial to promote the adsorption of Cr(VI) on biochar. It will not have adverse effects on the environment and organisms. However, up to now, there has been almost no research into the ecological remediation of heavy-metal-polluted water by PEG/MoS_2-modified biochar.

In this work, PEG was used as a surface modifier of MoS_2. It was loaded onto the surface of rice straw biochar to construct a highly efficient bio-adsorbent (PEG/MoS_2@BC) with an adjustable composition and controllable structure. Then, batch adsorption experiments under various conditions (altering the initial pH, dosage, initial concentration, contact time, and temperature) toward Cr(VI) in solution using PEG/MoS_2@BC were carried out to assess the influence of the operating parameters on the removal rate of Cr(VI) in solution. Finally, the micro-morphology and structure of PEG/MoS_2@BC were characterized *via* scanning electron microscopy (SEM), X-ray diffraction (XRD), Fourier-transform infrared spectroscopy (FT-IR), and X-ray photoelectron spectroscopy (XPS) to elucidate the reaction mechanism between PEG/MoS_2@BC and Cr(VI).

2 Materials and methods

2.1 Materials

Rice straw was purchased from a farm on the outskirts of Jinan, Shandong province, and then made into biochar. Polyethylene glycol (PEG) with a molecular weight of 400 Da (PEG 400) was purchased from Tianjin Institute of Photochemical Industry (Tianjin, China), ammonium molybdate ($(NH_4)_6Mo_7O_{24}\cdot 4H_2O$) was purchased from Tianjin Guangfu Technology Development Co., Ltd (Tianjin, China), sodium sulfide nonahydrate ($Na_2S\cdot 9H_2O$) was purchased from Shanghai Titan Science Co., Ltd (Shanghai, China), potassium dichromate ($K_2Cr_2O_7$, 99.8%) was purchased from Shanghai McLin Biotech Co., Ltd (Shanghai, China), 1,5-diphenylcarbohydrazide ($C_{13}H_{14}N_4O$) was purchased from National Pharmaceutical Group Chemical Reagent Co., Ltd (Shanghai, China), absolute ethanol (C_2H_6O) and sodium hydroxide (NaOH) were purchased from Guangdong Xilong Science Co., Ltd (Guangdong, China), and sulfuric acid (H_2SO_4) and hydrochloric acid (HCl) were purchased from Zhejiang Zhongxing Chemical Reagent Co., Ltd (Zhejiang, China). All reagents were analytical-grade and used without further purification. Distilled water was used to prepare all experimental solutions.

2.2 Preparation of PEG/MoS_2@BC

Rice straw, purchased from a farm in the suburbs of Jinan, Shandong province, was used as the raw material for the preparation of biochar *via* high-temperature pyrolysis. In short, the rice straw was dried in an oven at 110 °C. Then, it was washed for 10 min with a 10% HCl solution. 100 g of dried rice straw was crushed and screened to 200 mesh (particle size < 74 μm). It was calcined at 500 °C for 2 h in a low-oxygen muffle furnace to obtain rice straw biochar. A highly efficient

biosorption composite (PEG/MoS_2@BC) was constructed *via* the hydrothermal synthesis of MoS_2 with ammonium molybdate and sodium sulfide precursors, with the addition of appropriate amounts of PEG and rice straw biochar during the hydrothermal process. Specifically, 100 mL of 0.2 mol L^{-1} S^{2-} and 0.1 mol L^{-1} Mo^{2+} were added to a beaker, which was heated for 10 min. Then 5 g of biochar and 1 g of PEG 400 were added, and heating continued for 60 min. The whole mixture was heated in an electric furnace under stirring. During the heating process, distilled water was continuously added to maintain the volume of the solution at around 100 mL. Finally, the beaker was allowed to cool, and it was let stand until layers formed. The supernatant was removed and it was placed in a low-temperature drying oven to dry to a constant weight. As a result, PEG/MoS_2@BC was obtained. The synthesis procedure for the PEG/MoS_2@BC composite is displayed in Fig. 1.

2.3 Characterization techniques

SEM (Electronics company, Japan) was used for observing the surface morphology and structure of the adsorbent. At the end of SEM, the composition, distribution and content of elements in BC and the PEG/MoS_2@BC composite were determined based on energy dispersive spectroscopy (EDS) that was carried out at 20 kV. The functional group distribution on the surface of BC and the PEG/MoS_2@BC composite was analyzed using FT-IR spectroscopy (Nigoli, USA) in the wavenumber range of 400–4000 cm^{-1}. An Empyrean powder XRD diffractometer (Panalytical, Holland) was used to analyze the surface images of BC and the PEG/MoS_2@BC composite. All patterns were scanned at a rate of 3 s per step, and 2θ ranged from 10 to 60°. The electronic and chemical states of the samples were analyzed by XPS (Thermo Scientific K-Alpha, China). XPS data were assigned with the C 1s binding energy (284.80 eV) as the standard.[43]

2.4 Batch adsorption experiments with Cr(VI)

The effects of different factors on performance for the removal of Cr(VI) by PEG/MoS_2@BC were examined *via* batch experiments. 1 g L^{-1} Cr(VI) stock solution was prepared with $K_2Cr_2O_7$ crystals that were diluted to specific concentrations for investigation. The specific operations were as follows. Firstly, we prepared a certain concentration of Cr(VI) solution from the stock solution. Then, we measured 100 mL of Cr(VI) solution and poured it into a 250 mL conical flask. Subsequently, we added a certain amount of adsorbent into the 250 mL conical flask. Following this, we gently shook the 250 mL conical flask and replaced the stopper. Finally, we placed it in a thermostatic oscillation box. It was allowed to oscillate at 150 rpm. When the entire adsorption process reached equilibrium, the supernatant was collected and filtered through a 0.45 μm water filtration membrane. The concentration of Cr(VI) was determined using

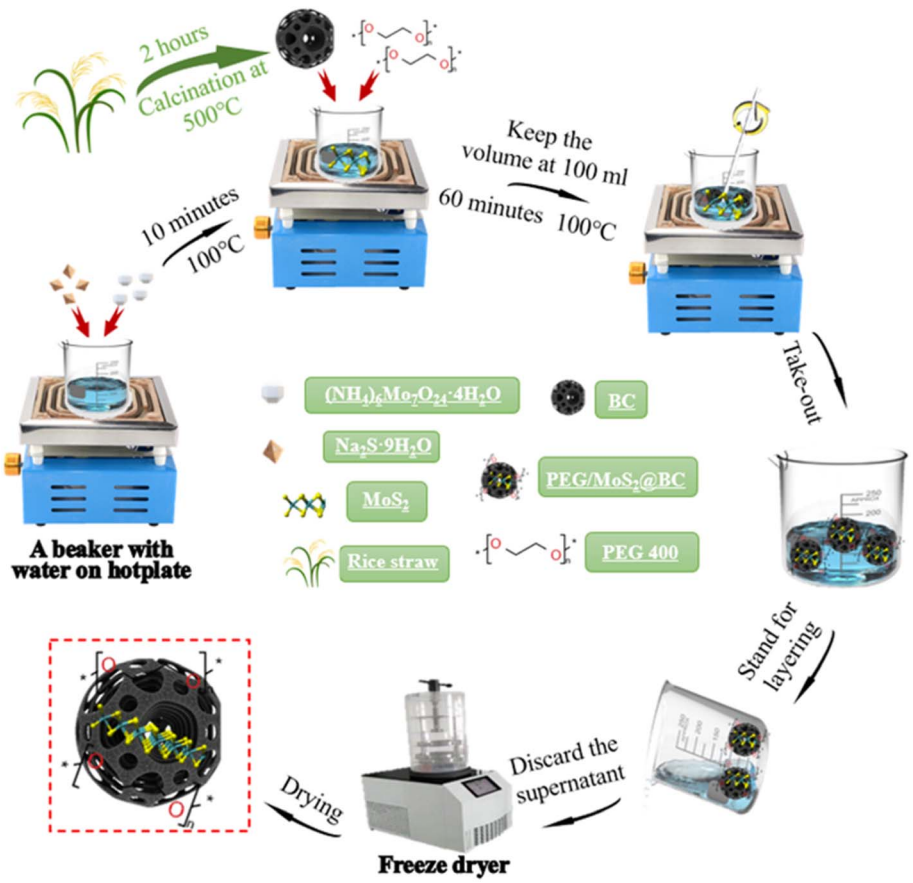

Fig. 1 The synthesis procedure for the PEG/MoS_2@BC composite.

a UV spectrometer (752N, INESA, Shanghai) at 540 nm *via* the 1,5-diphenylcarbohydrazide spectrophotometer method.[44] A blank control (no adsorbent added) was used to avoid the influence of precipitation on the adsorption process.

For the sake of our study, to examine the removal mechanism and characteristics of the adsorption process, the adsorption performance and behavior at different initial pH levels (2, 4, 6, 8, 10, and 12), initial concentrations (20 mg L^{-1}, 40 mg L^{-1}, 60 mg L^{-1}, 80 mg L^{-1}, and 100 mg L^{-1}), reaction times (5, 15, 30, 60, 90, 150, 210, 300, and 360 min) and temperatures (298.15 K, 308.15 K and 318.15 K) were investigated. The experiment was carried out by adding 0.1 g of PEG/MoS_2@BC into 100 mL of 20 mg L^{-1} Cr(VI) solution at an initial pH of 6 and reaction temperature of 308.15 K for a reaction time of 360 min. The residual Cr(VI) was determined based on the extraction of aliquots and filtration when the entire adsorption process reached equilibrium. The sorption isotherm of Cr(VI) solution at 298.15 K was analyzed, and the residual Cr(VI) was also determined based on the extraction of aliquots with filtration at several time points over 6 h. In addition, the removal rate (R (%)) and uptake capacity (q_e (mg g^{-1})) were calculated from the following eqn (1) and (2).

$$R\,(\%) = (C_0 - C_e)/C_0 \times 100\% \quad (1)$$

$$q_e\,(\text{mg g}^{-1}) = (C_0 - C_e) \times V/\text{m} \quad (2)$$

where C_0 and C_e represent the initial and equilibrium Cr(VI) concentrations in solution, respectively (mg L^{-1}), V is the volume of the solution (L), m is the mass of adsorbent (g) and q_e (mg g^{-1}) is the equilibrium sorption capacity.

2.5 Statistical analysis

Three parallel experiments were carried out to deal with the experimental data independently and repeatedly. The data were analyzed based on means and standard deviations. The figures were drawn based on the plotting function of Origin 2022. With this, the partial data obtained *via* the above experiments were linearly fitted using the ordinary least squares method. Significant difference analysis was applied using SPSS 25.0 statistical software. Statistical differences were considered significant at $P < 0.05$. The reaction kinetics data were fitted by the pseudo-first-order kinetics (eqn (3)) model and the pseudo-second-order kinetics model (eqn (4)). Adsorption isotherms were fitted using the Langmuir (eqn (5)) and the Freundlich (eqn (6)) isothermal models. Calculations of the thermodynamic parameters were done using eqn (7). The equations are as follows:

$$\lg(q_e - q_t) = \lg\ q_e - \frac{k_1 \times t}{2.303} \quad (3)$$

$$\frac{t}{q_t} = \frac{1}{k_2 \times q_e} + \frac{t}{q_e} \quad (4)$$

where q_t and q_e represent the adsorption capacity (mg g^{-1}) of the adsorbent at time t and equilibrium, respectively, and k_1 (min^{-1}) and k_2 (g mg^{-1} min^{-1}) represent the quasi-primary adsorption rate constant and the quasi-secondary adsorption rate constant, respectively. In addition:

$$\frac{C_e}{q_e} = \frac{1}{q_m \times K_L} + \frac{C_e}{q_m} \quad (5)$$

$$\ln\ q_e = \ln\ K_F + \frac{1}{n}\ln\ C_e \quad (6)$$

where q_e and q_m represent the equilibrium and saturated adsorption capacity (mg g^{-1}), respectively, C_e is the equilibrium adsorption concentration (mg L^{-1}), and K_L, K_F and n are the equilibrium adsorption constants (L mg^{-1}). Also:

$$\Delta G^\circ = -RT\ln\frac{q_e}{C_e} \quad (7)$$

$$\ln\frac{q_e}{C_e} = \frac{\Delta S^\circ}{R} - \frac{\Delta H^\circ}{RT} \quad (8)$$

where q_e represents the equilibrium adsorption capacity (mg g^{-1}), C_e is the equilibrium adsorption concentration (mg L^{-1}), ΔG° represents the change in Gibbs free energy under standard conditions (kJ mol^{-1}), T stands for temperature (K), R is the gas constant, and ΔH° and ΔS° are calculated from the slope and the intercept of related plots.

3 Results and discussion

3.1 Characterization of materials

The surface morphologies of biochar (BC) and the PEG/MoS_2@BC composite material were analyzed using SEM. Scanning electron micrographs of BC (Fig. 2(A)) and the PEG/MoS_2@BC composite material (Fig. 2(B)), magnified 5000 times, are shown in Fig. 2.

As shown in Fig. 2(A) and (B), significant differences in the external morphologies of BC and the PEG/MoS_2@BC composite material can be observed. The surface of the original BC was relatively smooth, with a flake-like structure of varying sizes and few surface pores. It is clearly shown (Fig. 2(B)) that many uniformly distributed strips of material (MoS_2) are present on the irregular surface of biochar. It can be observed that these are attached to the biochar, forming a rough surface. In the presence of PEG, the problem of the poor dispersion of MoS_2 was improved to some extent, reducing agglomeration while stabilizing MoS_2. This was consistent with the results of existing studies. Wu *et al.* found that when PEG was added, a large number of –OH functional groups were introduced, and nZVI was effectively dispersed on the BC surface.[42] It was shown that the strips on the surface of the biochar were MoS_2. The PEG and MoS_2 composite material was successfully loaded onto the biochar. PEG and biochar effectively increased the dispersion of MoS_2. Therefore, it is evident that a large amount of MoS_2 was loaded on the biochar, thereby increasing the contact area. This improved the biochar's ability to remove Cr(VI).

The EDS spectra of BC, PEG/MoS_2@BC and PEG/MoS_2@BC-Cr are shown in Fig. 3. BC is mainly composed of C and O elements, and the percentages of the two elements were 81.86% and 18.09%, respectively (Fig. 3(A)). Additionally, Mo (20.16%) and S (1.28%) were observed in PEG/MoS_2@BC along with C

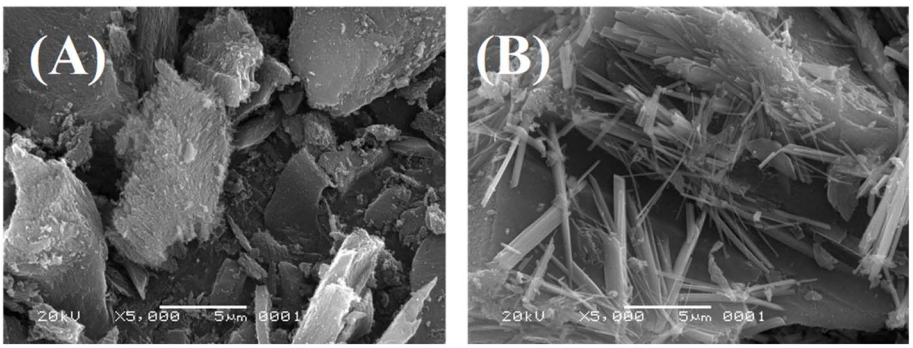

Fig. 2 SEM images of BC (A) and PEG/MoS_2@BC (B).

(63.25%) and O (14.91%) (Fig. 3(B)). The above elements were evenly distributed. This indicates that biochar serves as a scaffold material, uniformly loaded with Mo and S elements. Due to the large surface area of biochar and the ability of PEG to improve the dispersion of MoS_2, MoS_2 can be evenly attached to the surface of biochar. In other words, the preparation of PEG/MoS_2@BC has been proved to be successful, consistent with the results shown in Fig. 2. In addition to the four elements—C (80.29%), O (17.9%), Mo (0.98%) and S (0.55%)—Cr (0.18%) was observed in Fig. 3(C). This indicated that PEG/MoS_2@BC successfully adsorbed Cr(VI).

The crystal structures of BC and PEG/MoS_2@BC composites were analyzed based on X-ray diffraction patterns. The XRD spectra of BC and the PEG/MoS_2@BC composite are shown in Fig. 4. The black line in Fig. 4(A) shows the BC spectrum. It has two weak crystal diffraction peaks at 2θ values of 20.38° and 26.68°, which are similar to the typical structure of biochar.[45] In addition, a mild peak occurring at $2\theta = 27.52°$ might be due to the presence of inorganic Si elements from rice straw. In the PEG/MoS_2@BC spectrum (Fig. 4(A), blue line), typical diffraction peaks for MoS_2 appeared at 2θ values of 14.9°, 34.4°, and 56.74°, which represent the (002), (100), and (110) planes of MoS_2, respectively [PDF#37-1492].[46] This indicated that MoS_2 had been successfully loaded on the BC surface. After PEG@BC sulfation with MoS_2, the representative peaks of biochar at 20.38° and 26.68° disappeared because the biochar was covered by MoS_2. Some of the diffraction peaks elsewhere may be the result of interactions between biochar and MoS_2.

The FT-IR spectra of BC and the PEG/MoS_2@BC composite are shown in Fig. 4(B). For BC (Fig. 4(B), black line), there was an absorption peak at 518 cm^{-1}, which was caused by the C–O stretching vibration. The absorption peak at 1121 cm^{-1} was caused by the O–C–O stretching vibration. The absorption peak at 1384 cm^{-1} was caused by the C–OH stretching vibration.[47] The peak at 1626 cm^{-1} was caused by the C=C stretching vibration. The characteristic peak at 3421 cm^{-1} was attributed to the vibration of the –OH functional group.[48] PEG/MoS_2@BC contains the same functional groups as BC. However, compared with BC, PEG/MoS_2@BC has stronger intensities for each characteristic peak (Fig. 4(B), blue line). Among them, the enhancement of the characteristic peak of C–OH may be due to the addition of PEG, which increased the hydroxyl (–OH) content. This was consistent with the research results of Wu *et al.*[42] They found that when PEG was added to biochar, a large number of –OH functional groups could be introduced. The increase in C=O may be due to the formation of more C=O bonds due to high-temperature oxidation during the preparation of the composite. The rest of the characteristic peak changes may result from the interactions between biochar and MoS_2. Notably, the PEG/MoS_2@BC composite showed five new absorption peaks at 472.48 cm^{-1}, 617.12 cm^{-1}, 879.4 cm^{-1}, 1047.18 cm^{-1} and 2973.75 cm^{-1}. The peak at 472.48 cm^{-1}

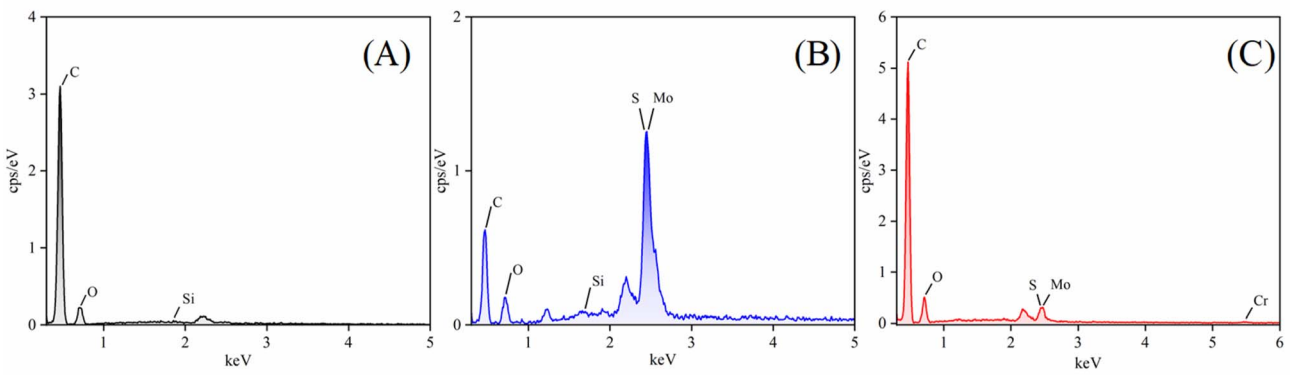

Fig. 3 EDS spectra of BC (A), PEG/MoS_2@BC (B), and PEG/MoS_2@BC-Cr (C).

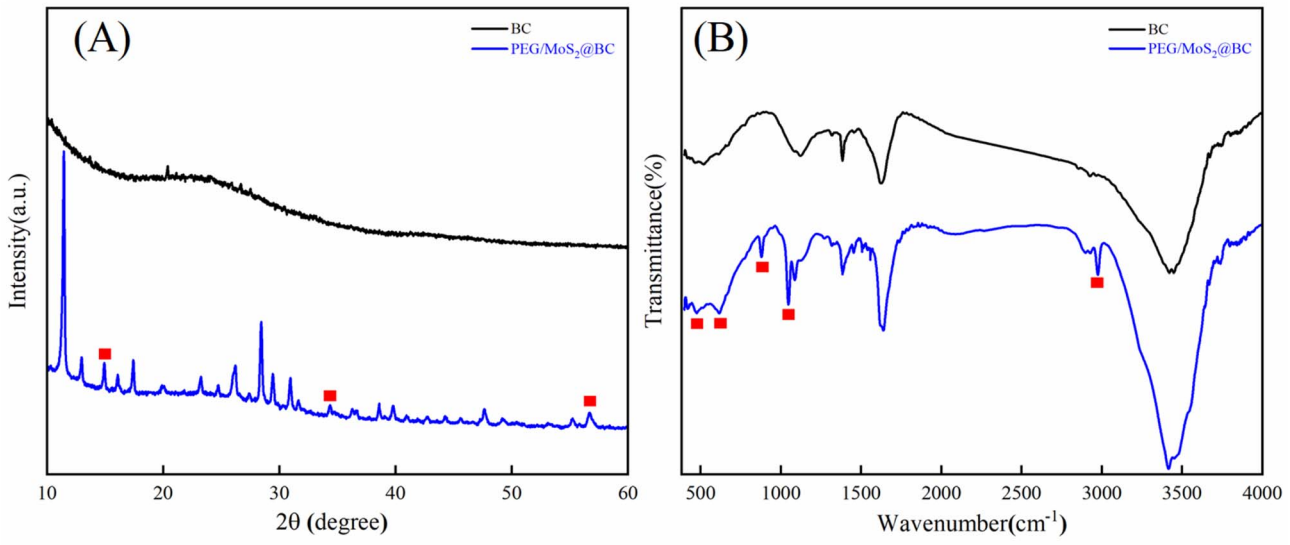

Fig. 4 XRD patterns (A) and FT-IR spectra (B) of biochar and PEG/MoS_2@BC.

should be the characteristic peak caused by the stretching vibration of Mo–S.[44] The absorption peak at 617.12 cm^{-1} may be caused by the stretching vibration of S–S. The characteristic peak of 879.4 cm^{-1} should be the characteristic peak caused by the stretching vibration of Mo–O. The peaks at 1047.18 cm^{-1} and 2973.75 cm^{-1} may be the result of the interaction between biochar and MoS_2. The results showed that a PEG/MoS_2@BC composite was successfully prepared, which was consistent with the characterization results described above.

3.2 Adsorption experiments

Fig. 5(A) shows the Cr(VI) removal rate of the PEG/MoS_2@BC composite as a function of contact time. When contact time increased, the adsorption capacity increased rapidly at first, then increased slowly. In this regard, it was speculated that active sites on the surface of the PEG/MoS_2@BC composite material were abundant in the initial stage of adsorption, and these then gradually decreased until saturation was reached.

The effect of experimental temperature on the removal rate of Cr(VI) is shown in Fig. 5(B). Within the temperature range of 298 K to 318 K, as the reaction temperature increased, the adsorption of Cr(VI) on the PEG/MoS_2@BC composite material improved. Experimental results have shown that at 298 K, the removal rate of Cr(VI) by the PEG/MoS_2@BC composite material was 77.68%, while at 318 K, the removal rate of Cr(VI) significantly increases to 89.56%. This may be because of the weak van der Waals forces between the layers of MoS_2, facilitating easy interlayer sliding. An increase in temperature resulted in an increase in the interlayer spacing of MoS_2. As the layer spacing increased, more Cr(VI) could be adsorbed into the intermediate layers of MoS_2.

The pH of the solution controlled the adsorption process of Cr(VI) by affecting the dissociation state of surface functional groups of the solid adsorbent and the surface charge distribution, as well as the valence state of Cr(VI) in solution. The influence of pH on the adsorption of Cr(VI) by PEG/MoS_2@BC is shown in Fig. 5(C). As the pH increased, the removal rate of Cr(VI) by PEG/MoS_2@BC gradually decreased, which was consistent with the results of previous studies.[47,49] Because PEG is stable over a wide pH range, it is not susceptible to environmental factors such as acids and alkalis. Thus, the dispersion of MoS_2 on the BC surface was maintained. The PEG/MoS_2@BC composite was ensured to have abundant adsorption sites. Additionally, at low-pH, the surface of MoS_2 was rich in sulfide groups with Lewis basicity. They can serve as active sites that selectively bind to metals, effectively adsorbing Cr(VI). As the pH of the solution increases, the sulfur-containing functional groups deprotonate. Thus, the PEG/MoS_2@BC composite material becomes negatively charged. As a result, electrostatic repulsion occurred between Cr(VI) and the PEG/MoS_2@BC composite material, ultimately reducing the removal efficiency of Cr(VI). Therefore, at low pH, the PEG/MoS_2@BC composite showed better Cr(VI) removal performance.

The adsorption of Cr(VI) by the PEG/MoS_2@BC composite material was influenced by the initial concentration of Cr(VI), as shown in Fig. 5(D). As can be seen from Fig. 5(D), at 298 K, as the concentration of Cr(VI) increased, the removal rate of Cr(VI) from solution also increased. This may be due to the increased concentration of Cr(VI) in the aqueous solution, which increased the chance of Cr(VI) collision with the PEG/MoS_2@BC composite.

3.3 Adsorption kinetics, adsorption isotherms and thermodynamics

To investigate the mechanism of adsorption, we employed the pseudo-first-order kinetic model (PFO) and pseudo-second-order kinetic model (PSO) to fit the adsorption data. The kinetics fitting curves for Cr(VI) ions in PEG/MoS_2@BC solution are shown in Fig. 6(A) and (B).

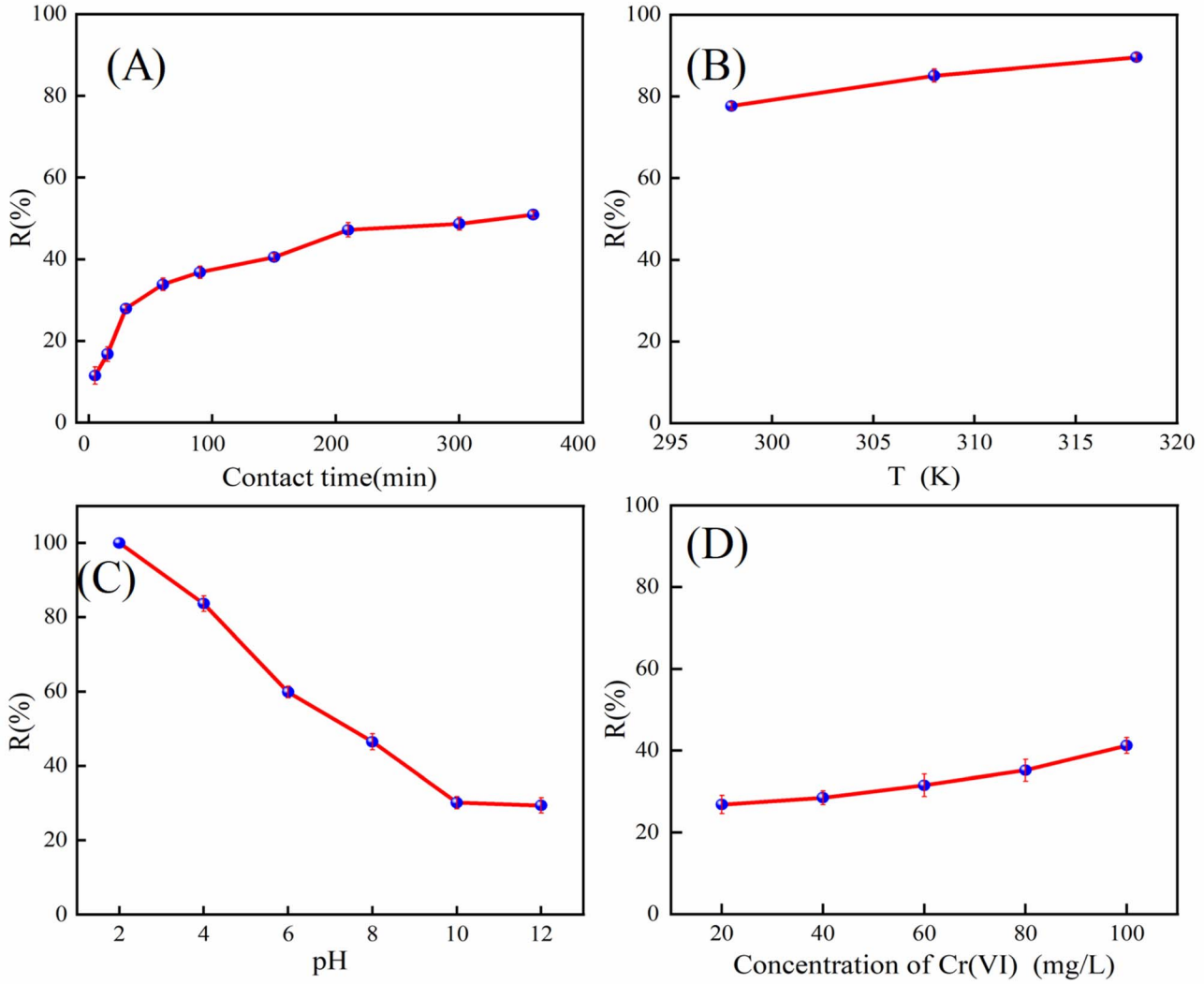

Fig. 5 Effects of the operational parameters on Cr(VI) removal in solution: (A) contact time; (B) temperature; (C) pH; and (D) concentration of Cr(VI).

Kinetics curves of the adsorption of Cr(VI) in solution on PEG/MoS_2@BC are described in Fig. 6(A) and (B). The results showed that the correlation coefficient of the pseudo-second-order kinetic model ($R^2 = 0.9944$) was higher than that of the pseudo-first-order kinetic model ($R^2 = 0.9620$). Therefore, the adsorption process of Cr(VI) on PEG/MoS_2@BC can be better described using the pseudo-second-order model. It was suggested that the adsorption process of Cr(VI) on PEG/MoS_2@BC should involve chemical reactions, such as mineral precipitation, surface complexation, or cation exchange. The adsorption reaction is usually a comprehensive process involving multiple steps. Therefore, we further analyzed the steps of the Cr(VI) adsorption process using the intraparticle diffusion model (IPD). As shown in Fig. 7 and Table 1, the graph of the intraparticle diffusion model exhibits a three-stage linear relationship. None of the three segments passes through the origin. This indicated that surface diffusion was not the only limiting step in the adsorption process of Cr(VI) on PEG/MoS_2@BC. The linear coefficients (R^2) for the three stages were all greater than 0.91. This indicated that the adsorption process of Cr(VI) consists of multiple steps. The rate constants for the three stages are in the order K1 > K2 > K3. It is suggested that as time increased, the adsorption sites on the PEG/MoS_2@BC composite material were occupied by Cr(VI), and then the diffusion rate gradually slowed down. The first stage was generally considered as a surface diffusion stage, where the adsorption sites on the surface of the PEG/MoS_2@BC composite material react with Cr(VI). The second stage was believed to be an intraparticle diffusion stage. The third stage was considered to be a micropore diffusion stage. After surface adsorption saturation, the particles diffuse into the interstices of the PEG/MoS_2@BC composite material. Compared to surface adsorption, the occurrence of the adsorption reaction becomes difficult. The diffusion rate gradually decreases until adsorption equilibrium is reached. The C value represents the diffusion resistance, which increased gradually from the first stage to the third stage. This indicated that the increase in diffusion resistance would hinder the internal diffusion of particles.[50–52]

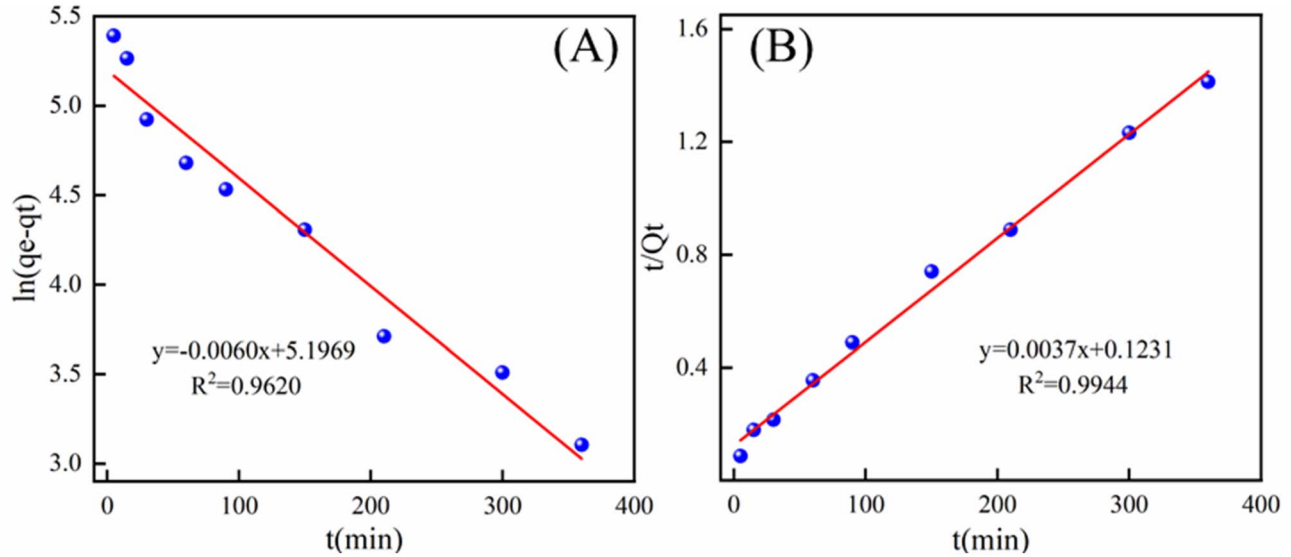

Fig. 6 The kinetics for the adsorption of Cr(VI) by PEG/MoS_2@BC: (A) pseudo-first-order kinetic model; and (B) pseudo-second-order kinetic model.

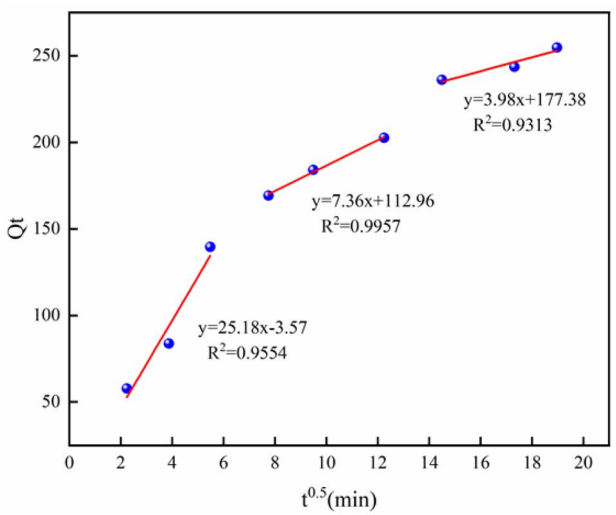

Fig. 7 The intraparticle diffusion model for Cr(VI) on PEG/MoS_2@BC.

Therefore, surface diffusion was not the only step. It was accompanied by intraparticle diffusion and micropore diffusion of the particles.

The adsorption isotherm can provide important information about the surface properties and adsorption mechanisms of adsorbents. As shown in Fig. 8(A) and (B), the adsorption of Cr(VI) by PEG/MoS_2@BC was fitted using the Langmuir and Freundlich isotherm models to characterize the adsorption behavior of PEG/MoS_2@BC towards Cr(VI) ions in solution. The results indicated that the linear correlation coefficient of the Langmuir model (R^2 = 0.9314) was higher than that of the Freundlich model (R^2 = 0.8383). Therefore, the Langmuir model can effectively depict the adsorption process of Cr(VI) on PEG/MoS_2@BC. This shows that the adsorption of Cr(VI) on PEG/MoS_2@BC was mainly controlled by monolayer chemisorption.[53] It was also indicated that the q value calculated *via* the Langmuir isotherm model was closer to the experimental adsorption data.

To further investigate the influence of temperature on the adsorption performance of PEG/MoS_2@BC toward Cr(VI) and the adsorption mechanism, thermodynamic equations were used to evaluate the data. The results are shown in Table 2. It is shown that the Gibbs free energy (ΔG°) at all three temperatures was negative. This indicated that the adsorption process of Cr(VI) ions (in solution) on PEG/MoS_2@BC is spontaneous under the experimental conditions.[42] Meanwhile, the value of ΔG° decreased as the reaction temperature increased. This also confirms the experimental results showing that an increase in temperature enhances the adsorption of Cr(VI) by the PEG/MoS_2@BC composite material. The value of ΔH° was 514.85 kJ mol^{-1}. The positive enthalpy change indicated that the adsorption process was endothermic. The value of ΔS° was 129.86 J mol^{-1} K^{-1}. ΔS° reflects the disorder at the solid–liquid

Table 1 The IPD parameters for Cr(VI) on PEG/MoS_2@BC

K1 mg g^{-1} $min^{0.5}$	C1 mg g^{-1}	R^2	K2 mg g^{-1} $min^{0.5}$	C2 mg g^{-1}	R^2	K3 mg g^{-1} $min^{0.5}$	C3 mg g^{-1}	R^2
25.18	−3.57	0.9554	7.36	112.96	0.9957	3.98	177.38	0.9313

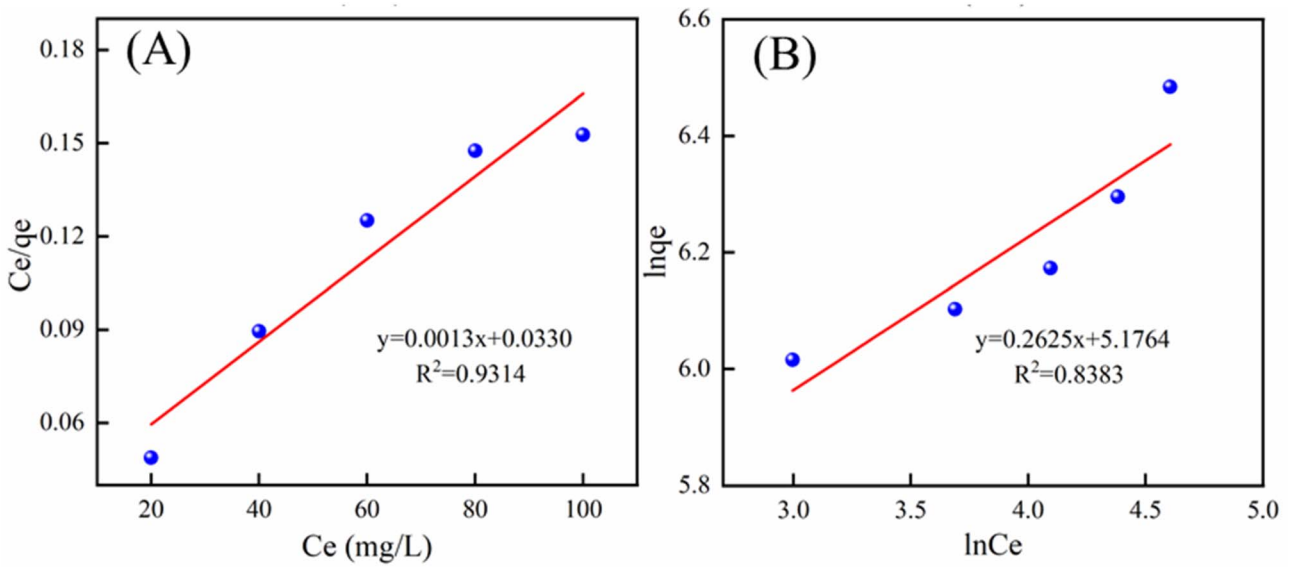

Fig. 8 The adsorption isotherms for Cr(VI) on PEG/MoS_2@BC: (A) the Langmuir isotherm model; and (B) the Freundlich isotherm model.

Table 2 The thermodynamic parameters of Cr(VI) adsorption on PEG/MoS_2@BC

$\Delta G°$ (kJ mol^{-1})			$\Delta H°$	$\Delta S°$	
298 K	308 K	318 K	(kJ mol^{-1})	(J mol^{-1} K^{-1})	R^2
−3.09	−4.46	−5.68	514.85	129.86	0.9985

interface.[54] In conclusion, the adsorption process of Cr(VI) by PEG/MoS_2@BC was spontaneous and endothermic.

3.4 Reaction mechanism

In order to further study the possible adsorption mechanism of Cr(VI) removal, XPS analysis was used to analyze the valence changes of the main elements before and after adsorption. Fig. 9 shows the XPS full-scan spectra of PEG/MoS_2@BC before and after the adsorption of Cr(VI). The main elements were C, O, S, and Mo. The four peaks at 284.8 eV, 531.22 eV, 233.1 eV, and 164.22 eV were assigned to C 1s, O 1s, Mo 3d, and S 2p, respectively. Their proportions were 75.15%, 20.31%, 2.45% and 2.09%, respectively. However, after the adsorption of Cr(VI), the Mo 3d peak was significantly weakened, the O 1s peak was slightly weakened, the C 1s peak was slightly enhanced, the S 2p remained almost unchanged, and Cr 2p showed a weak peak at 581.04 eV (Fig. 9, red line). After the adsorption of Cr(VI), the proportions of C, O, Mo and S were 81.47%, 15.58%, 0.63% and 2.00%, respectively, with the remainder being Cr. The appearance of Cr 2p indicated that Cr was efficiently deposited on the PEG/MoS_2@BC surface.[52]

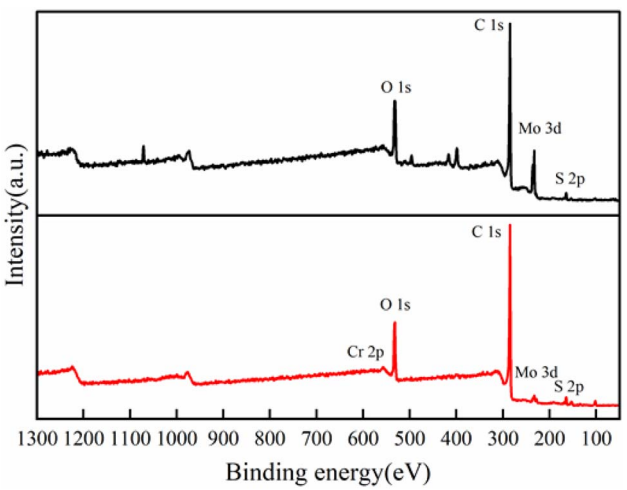

Fig. 9 XPS survey spectra of samples before (black) and after (red) Cr(VI) adsorption.

The C 1s XPS spectra before and after adsorption are shown in Fig. 10(A). The C 1s spectra were mainly composed of three peaks, at 284.80 eV, 286.31 eV, and 287.74 eV, which were attributed to C═C, C–O, and C═O, respectively. These were the main functional groups of PEG/MoS_2@BC. The negatively charged peaks at 531.22 eV and 533.08 eV in the O 1s spectra (Fig. 10(B)) were assigned to oxide (O^{2-}) and surface hydroxyl (–OH) groups, respectively.[53] After the adsorption of Cr(VI), the –OH content increased from 58.47% to 63.38%. This indicated the formation of the corresponding hydroxide, that is, the reduction reaction occurred to form $Cr(OH)_3$ (Cr(VI) → Cr(III)).[55]

The S 2p XPS spectra of PEG/MoS_2@BC are shown in Fig. 10(C). As seen, the characteristic peaks at 164.08 eV and 165.24 eV were attributed to S^{2-} $2p_{3/2}$ and S^{2-} 2p, respectively. The characteristic peaks at 168.03 eV and 170.33 eV were assigned to SO_4^{2-} $2p_{3/2}$ and SO_4^{2-} $2p_{1/2}$, respectively.[44] After the adsorption of Cr(VI), the electron binding energies of the S^{2-} $2p_{3/2}$ and S^{2-} $2p_{1/2}$ orbitals of PEG/MoS_2@BC increased by 0.07 and 0.19 eV, respectively. The results showed that MoS_2 donated electrons, which helped in the reduction of Cr(VI) to Cr(III).

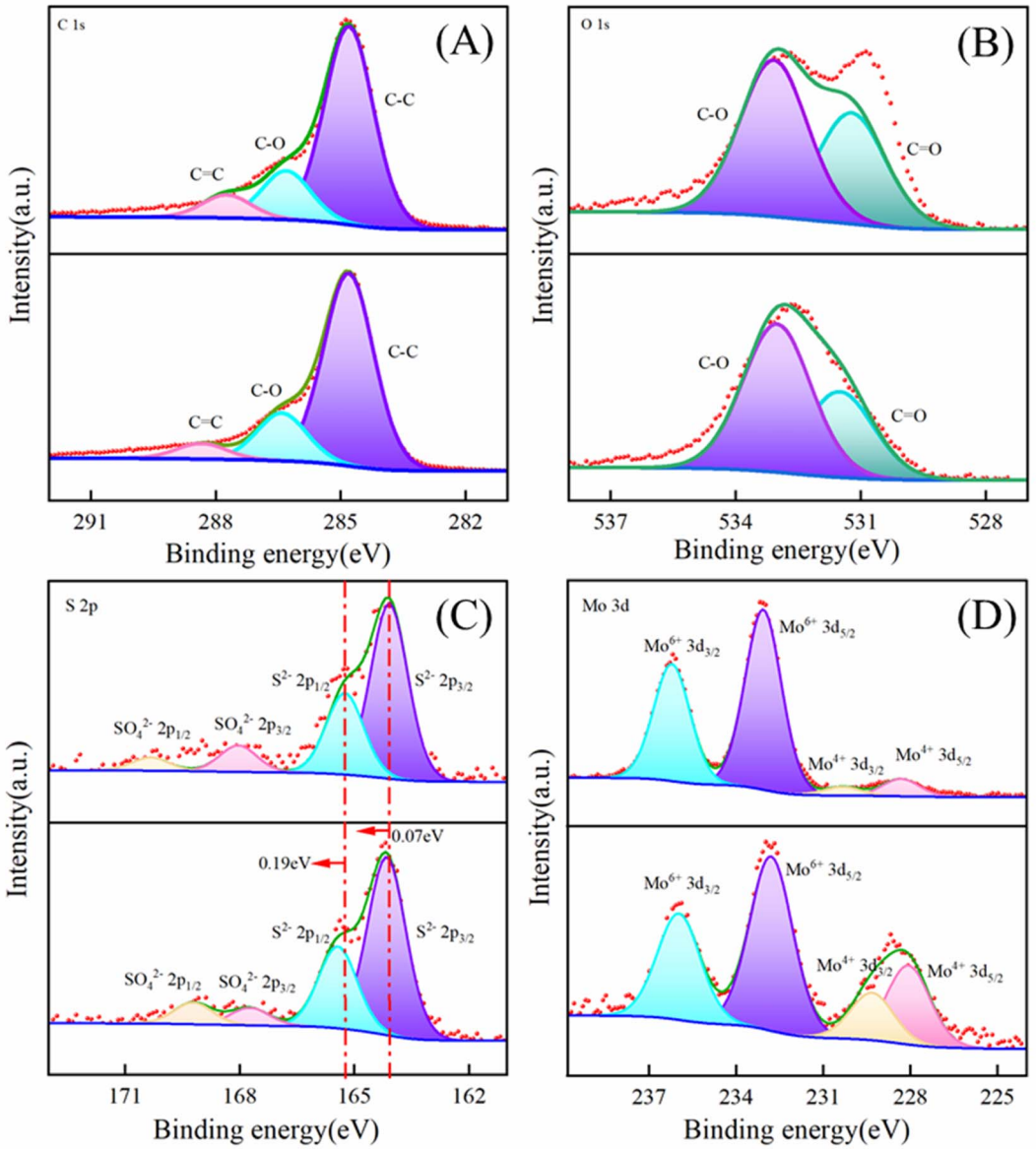

Fig. 10 XPS spectra of PEG/MoS_2@BC before (top) and after (bottom) Cr(VI) adsorption: (A) C 1s, (B) O 1s, (C) S 2p and (D) Mo 3d.

Fig. 10(D) shows the Mo 3d XPS spectra of PEG/MoS_2@BC. Here, the characteristic peaks at 228.32 eV and 230.34 eV were attributed to Mo^{4+} $3d_{5/2}$ and Mo^{4+} $3d_{3/2}$ from MoS_2, respectively. The characteristic peaks at 233.06 eV and 236.21 eV were attributed to Mo^{6+} $3d_{5/2}$ and Mo^{6+} $3d_{3/2}$ from MoO_4^{2-}, respectively.[35,54] The overall content of Mo on the surface decreased after the adsorption of Cr(VI). The amount of Mo(VI) decreased from 91.86% to 68.92%. The proportion of Mo(IV) was elevated. Combined with the increase in the content of –OH after the adsorption of Cr(VI) seen in Fig. 10(B), this indicated that Mo was involved in the ionic redox reaction of Cr(VI).

According to the characterization experiments, including SEM, EDS, XRD, FTIR and XPS, it can be observed that the surface of PEG/MoS_2@BC was irregular and rough. MoS_2 was dispersed on the BC surface. Alkoxyl C–O, carboxyl O=C–O, C=C, C≡C, and –OH functional groups exist on the surface of PEG/MoS_2@BC. Cr(VI) ions in solution can form complexes with Cr(VI) through hydrogen bonding and functional groups, fixing Cr(VI) on the adsorbent surface. Particularly, under acidic conditions, Cr(VI) was easily reduced to Cr(III) upon gaining electrons. Furthermore, the porous structure and large specific surface area of the PEG/MoS_2@BC composite material provide sites for the physical adsorption of Cr(VI). The material adsorbs Cr(VI) through pores filled with adsorbent. Meanwhile, in the low-pH system, the surface of MoS_2 was rich in sulfide groups with Lewis basicity. They can serve as active sites to selectively bind metals, effectively adsorbing Cr(VI). Therefore, this study proposed that the reaction mechanism by which PEG/MoS_2@BC removes Cr(VI) mainly includes electron attraction, reduction reactions, complexation, and physical adsorption. The adsorption mechanism of Cr(VI) on the adsorbent is shown in Fig. 11.

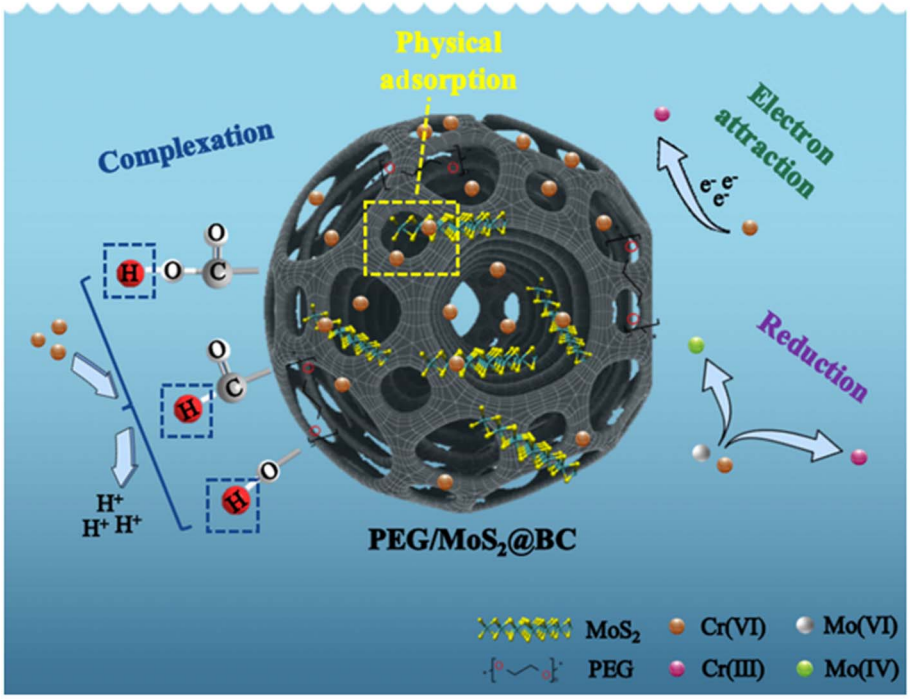

Fig. 11 The adsorption mechanism of Cr(VI) on the adsorbent.

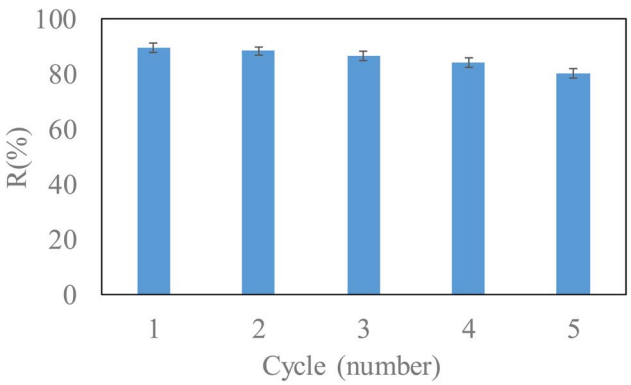

Fig. 12 The regeneration of PEG/MoS_2@BC for Cr(VI) removal (reaction conditions: dosage of PEG/MoS_2@BC, 0.1 g L^{-1}; reaction time, 360 min; initial concentration of Cr(VI), 20 mg L^{-1}; temperature, 318.15 K; solution pH, 6).

3.5 Recycling experiments

In order to assess the sustainability and economic viability of the prepared adsorbent, the regeneration and reusability of PEG/MoS_2@BC were investigated. Regeneration refers to the restoration of the adsorbent's capacity to sequester contaminants, particularly after it has reached saturation with heavy metals. In this work, recycling experiments involving PEG/MoS_2@BC were carried out over consecutive cycles. The reaction conditions were as follows: 0.1 g of PEG/MoS_2@BC, 20 mg L^{-1} of Cr(VI), an initial pH of 6, a temperature of 318.15 K and a reaction time of 360 min. Here, we employed a chemical washing method using acidic solution to effectively displace Cr(VI) ions from the adsorption sites. This could be because there was repulsion at acidic pH between protonated amine groups and metallic ions that increased the process of desorption. According to related research, nitric acid was established as the optimal choice.[47] PEG/MoS_2@BC, after the adsorption of Cr(VI), was soaked in 100 mL of 5% HNO_3 solution for 48 h. The results of recycling experiments are described in Fig. 12.

As the cycle number increased, the adsorption capacity for Cr(VI) of PEG/MoS_2@BC decreased slowly. Several factors contributed to the reduced adsorption efficiency post-regeneration, among which structural degradation, a loss of functional groups, residual uranium ions, and alterations in surface properties are paramount. The adsorption capacity of Cr(VI) decreases from 89.56% to 80.14% over five adsorption and desorption cycles. The fifth cycle exhibited only a slight decline in adsorption capacity, registering a minimal loss of just 9.42%. When the number of adsorption cycles was five, the adsorption capacity for Cr(VI) of PEG/MoS_2@BC still reached 80.14%. Notably, the fifth cycle exhibited only a slight decline in adsorption capacity. This implies that the PEG/MoS_2@BC is chemically stable and reusable for wastewater treatment at low replacement cost.

4 Conclusions

PEG and MoS_2 were successfully loaded onto biochar prepared from rice straw. PEG and biochar effectively reduced the aggregation of MoS_2, resulting in the preparation of an efficient bio-adsorbent (PEG/MoS_2@BC). The adsorption process of Cr(VI) ions on PEG/MoS_2@BC conforms more to the Langmuir isotherm model and pseudo-second-order kinetic model. In

other words, the removal of Cr(VI) by PEG/MoS_2@BC was closer to a chemical reaction and primarily involved monolayer adsorption. The adsorption of Cr(VI) ions from solution by PEG/MoS_2@BC was spontaneous and endothermic. The proposed reaction mechanism for the removal of Cr(VI) ions by PEG/MoS_2@BC mainly includes complexation reactions, reduction reactions, ion–exchange reactions, and physical adsorption. The adsorption material PEG/MoS_2@BC exhibited high reusability and stability. This study provides a new approach for environmental pollutant remediation using modified biochar.

Conflicts of interest

There are no conflicts to declare.

Data availability

The data and materials presented in this study are available on request from the corresponding author. The data are not publicly available due to privacy restrictions.

Acknowledgements

This work was supported by the Science and Technology Plan Project of Shaoxing (2024001020).

References

1 S. Li, W. Wang, Y. Liu and W. Zhang, Zero-valent iron nanoparticles (nZVI) for the treatment of smelting wastewater: A pilot-scale demonstration, *Chem. Eng. J.*, 2014, **254**, 115–123.
2 V. Sarin, T. S. Singh and K. K. Pant, Thermodynamic and breakthrough column studies for the selective sorption of chromium from industrial effluent on activated eucalyptus bark, *Bioresour. Technol.*, 2006, **97**, 1986–1993.
3 M. Deng, X. Wang, Y. Li, F. Wang, Z. Jiang, Y. Liu, Z. Gu, S. Xia and J. Zhao, Reduction and immobilization of Cr(VI) in aqueous solutions by blast furnace slag supported sulfidized nanoscale zerovalent iron, *Sci. Total Environ.*, 2020, **743**, 140722.
4 S. Youcef, M. Chebbi, L. Youcef, M. G. Bouaziz, A. Soudani, A. Sahli and C. Deroues, Chemical oxygen demand (COD) reduction in wastewater from the textile industry by coagulation-flocculation and adsorption, *Environ. Monit. Assess.*, 2025, **197**, 536.
5 J. Wei, Y. Duan, M. Li, H. Lin, J. Lv, Z. Chen, J. Lin, H. Song, R. Zhang, L. Li and L. Huang, A novel manganese sulfide encapsulating biochar-dispersed zero-valent iron composite for high removal ability of Cr(VI) in water and its mechanism, *Colloids Surf., A*, 2023, **658**, 130556.
6 S. Liu, K. Chen, H. Xiao, Z. Chen, S. Zhang, H. Ding and L. Yang, Efficient reduction of Cr(VI) and elimination of total Cr with S-bridged Ni_3S_2/MoS_2 nanowire electrode, *J. Environ. Chem. End.*, 2023, **11**, 109647.
7 T. Ge, Z. Jiang, L. Shen, J. Li, Z. Lu, Y. Zhang and F. Wang, Synthesis and application of $Fe_3O_4/FeWO_4$ composite as an efficient and magnetically recoverable visible light-driven photocatalyst for the reduction of Cr(VI), *Sep. Purif. Technol.*, 2021, **263**, 118401.
8 S. Youcef, S. Guergazi and L. Youcef, Adsorption modeling of Cu and Zn in single and combined systems onto activated carbon of olive stone, *Model. Earth Syst. Environ.*, 2022, **8**, 3927–3940.
9 C. Ramakrishnaiah and A. Prathima, Hexavalent chromium removal from industrial wastewater by chemical precipitation method, *Int. J. Appl. Eng. Res.*, 2012, **2**, 599–603.
10 Q. Cheng, C. Wang, K. Doudrick and C. K. Chan, Hexavalent chromium removal using metal oxide photocatalysts, *Appl. Catal., B*, 2015, **176**, 740–748.
11 Y. Xie, J. Lin, J. Liang, M. Li, Y. Fu, H. Wang, S. Tu and J. Li, Hypercrosslinked mesoporous poly (ionic liquid) s with high density of ion pairs: Efficient adsorbents for Cr(VI) removal *via* ion-exchange, *Chem. Eng. J.*, 2019, **378**, 122107.
12 P. Lakshmipathiraj, G. B. Raju, M. R. Basariya, S. Parvathy and S. Prabhakar, Removal of Cr(VI) by electrochemical reduction, *Sep. Purif. Technol.*, 2008, **60**, 96–102.
13 C. Shen, H. Chen, S. Wu, Y. Wen, L. Li, Z. Jiang, M. Li and W. Liu, Highly efficient detoxification of Cr(VI) by chitosan–Fe(III) complex: Process and mechanism studies, *J. Hazard. Mater.*, 2013, **244**, 689–697.
14 M. B. Ahmed, J. L. Zhou, H. H. Ngo, W. Guo and M. Chen, Progress in the preparation and application of modified biochar for improved contaminant removal from water and wastewater, Bioresource, *Technol*, 2016, **214**, 836–851.
15 P. Wu, S. T. Ata-Ul-Karim, B. P. Singh, H. Wang, T. Wu, C. Liu, G. Fang, D. Zhou, Y. Wang and W. Chen, A scientometric review of biochar research in the past 20 years(1998–2018), *Biochar*, 2019, **1**, 23–43.
16 C. Wang, L. Gu, S. Ge, X. Liu, X. Zhang and X. Chen, Remediation potential of immobilized bacterial consortium with biochar as carrier in pyrene-Cr(VI) co-contaminated soil, *Environ. Technol.*, 2019, **40**, 2345–2353.
17 S. Wang, B. Gao, Y. Li, A. E. Creamer and F. He, Adsorptive removal of arsenate from aqueous solutions by biochar supported zero-valent iron nanocomposite: batch and continuous flow tests, *J. Hazard. Mater.*, 2017, **322**, 172–181.
18 A. Soudani, L. Youcef, L. Bulgariu, S. Youcef, K. Toumi and N. Soudani, Characterizing and modeling of oak fruit shells biochar as an adsorbent for the removal of Cu, Cd, and Zn in single and in competitive systems, *Chem. Eng. Res. Des.*, 2022, **188**, 972–987.
19 A. Soudani, L. Youcef, S. Youcef, S. Elbahi, K. Toumi, G. Saadia, A. Sahli and N. Soudani, High Performance Activated Carbon Based on Date Palm Fibers for Cu^{2+} Removal in Water, *Chem. Afr.*, 2024, **7**, 3903–3915.
20 M. Chebbi, S. Youcef, L. Youcef, A. Soudani, C. Dridi, A. Sahli, A. Houchet and C. Deroues, Single and combined treatment processes for rhodamine B removal by coagulation–flocculation and adsorption, *RSC Adv.*, 2024, **14**, 37833–37845.
21 D. Mohan, A. Sarswat, Y. S. Ok and C. U. Pittman, Organic and inorganic contaminants removal from water with

biochar, a renewable, low cost and sustainable adsorbent–a critical review, *Bioresour. Technol.*, 2014, **160**, 191–202.

22 H. Li, S. A. A. Mahyoub, W. Liao, S. Xia, H. Zhao, M. Guo and P. Ma, Effect of pyrolysis temperature on characteristics and aromatic contaminants adsorption behavior of magnetic biochar derived from pyrolysis oil distillation residue, *Bioresour. Technol.*, 2017, **223**, 20–26.

23 L. L. Ling, W. J. Liu, S. Zhang and H. Jiang, technology, Magnesium oxide embedded nitrogen self-doped biochar composites: fast and high-efficiency adsorption of heavy metals in an aqueous solution, *Environ. Sci. Technol.*, 2017, **51**, 10081–10089.

24 T. Zhou, M. Zhao, X. Zhao, Y. Guo and Y. Zhao, Simultaneous remediation and fertility improvement of heavy metals contaminated soil by a novel composite hydrogel synthesized from food waste, *Chemosphere*, 2021, **275**, 129984.

25 Y. Liu, S. P. Sohi, S. Liu, J. Guan, J. Zhou and J. Chen, Adsorption and reductive degradation of Cr(VI) and TCE by a simply synthesized zero valent iron magnetic biochar, *J. Environ. Manage.*, 2019, **235**, 276–281.

26 B. Qiu, X. Tao, H. Wang, W. Li, X. Ding and H. Chu, A Pyrolysis, Biochar as a low-cost adsorbent for aqueous heavy metal removal: A review, *J. Anal. Appl. Pyrolysis*, 2021, **155**, 105081.

27 H. N. Tran, S. J. You, B. A. Hosseini and H. P. Chao, Mistakes and inconsistencies regarding adsorption of contaminants from aqueous solutions: A critical review, *Water Res.*, 2017, **120**, 88–116.

28 H. S. Benammar, S. Guergazi, S. Youcef and L. Youcef, Removal of Congo red and Naphthol blue black dyes from aqueous solution by adsorption on activated carbon. Characterization, kinetic and equilibrium in nonlinear models studies, *Desalination Water Treat.*, 2021, **221**, 3.

29 K. N. Palansooriya, J. T. F. Wong, Y. Hashimoto, L. Huang, J. Rinklebe, S. X. Chang, N. Bolan, H. Wang and Y. S. Ok, Response of microbial communities to biochar-amended soils: a critical review, *Biochar*, 2019, **1**, 3–22.

30 S. Zhu, S.-H. Ho, X. Huang, D. Wang, F. Yang, L. Wang, C. Wang, X. Cao and F. Ma, Magnetic nanoscale zerovalent iron assisted biochar: interfacial chemical behaviors and heavy metals remediation performance, *ACS Sustainable Chem. Eng.*, 2017, **5**, 9673–9682.

31 X. Li, C. Wang, J. Zhang, J. Liu, B. Liu and G. Chen, Preparation and application of magnetic biochar in water treatment: a critical review, *Sci. Total Environ.*, 2020, **711**, 134847.

32 Q. Chen, J. Zheng, Q. Yang, Z. Dang and L. Zhang, Insights into the glyphosate adsorption behavior and mechanism by a $MnFe_2O_4$@cellulose-activated carbon magnetic hybrid, *Sci. Total Environ.*, 2019, **11**, 15478–15488.

33 J. Y. Kim, S. Oh and Y. K. Park, Overview of biochar production from preservative-treated wood with detailed analysis of biochar characteristics, heavy metals behaviors, and their ecotoxicity, *J. Hazard. Mater.*, 2020, **384**, 121356.

34 Y. Venkata Subbaiah, K. Saji and A. Tiwari, Atomically thin MoS_2: a versatile nongraphene 2D material, *Adv. Funct. Mater.*, 2016, **26**, 2046–2069.

35 E. Hu, E. Su, Y. Chen, A. Subedi, J. Wang, K. Hu, X. Hu and L. Tang, Preparation and Tribological behaviors of modified Rice husk carbon/MoS_2 composite particles as a functional additive in polyethylene glycol, *J. Environ. Chem. Eng.*, 2022, **65**, 564–577.

36 T. Liu, J. Qin, J. Wang and J. Li, On the tribological properties of RGO–MoS_2 composites surface modified by oleic acid, *Tribol. Lett.*, 2022, **70**, 14.

37 Z. Chen, H. Yan, T. Liu and S. Niu, Nanosheets of MoS_2 and reduced graphene oxide as hybrid fillers improved the mechanical and tribological properties of bismaleimide composites, *Compos. Sci. Technol.*, 2016, **125**, 47–54.

38 R. Zhao, M. Lv, Y. Li, M. Sun, W. Kong, L. Wang, S. Song, C. Fan, L. Jia and S. Qiu, Stable nanocomposite based on PEGylated and silver nanoparticles loaded graphene oxide for long-term antibacterial activity, *ACS Appl. Mater. Interfaces*, 2017, **9**, 15328–15341.

39 A. H. Keihan, H. Veisi and P. M. Biabri, Facile synthesis of PEG-coated magnetite (Fe_3O_4) and embedment of gold nanoparticle as a nontoxic antimicrobial agent, *Chemosphere*, 2017, **31**, 3873.

40 H. Tian, Y. Liang, T. Zhu, X. Zeng and Y. Sun, Surfactant-enhanced PEG-4000-NZVI for remediating trichloroethylene-contaminated soil, *Chemosphere*, 2018, **195**, 585–593.

41 W. M. Obeidat and A. S. A. Sallam, Evaluation of tadalafil nanosuspensions and their PEG solid dispersion matrices for enhancing its dissolution properties, *AAPS PharmSciTech*, 2014, **15**, 364–374.

42 H. Wu, W. Wei, C. Xu, Y. Meng, W. Bai, W. Yang, A. Lin and E. Safety, Polyethylene glycol-stabilized nano zero-valent iron supported by biochar for highly efficient removal of Cr(VI), *Ecotoxicol. Environ. Saf.*, 2020, **188**, 109902.

43 L. Han, H. Sun, K. Sun, Y. Yang, L. Fang and B. Xing, Effect of Fe and Al ions on the production of biochar from agricultural biomass: properties, stability and adsorption efficiency of biochar, *Renewable Sustainable Energy Rev.*, 2021, **145**, 111133.

44 J. Ma, N. Jia, H. Jin, S. Yao, K. Zhang, Y. Kai, W. Wu and Y. Wen, Chitosan induced synthesis of few-layer MoS_2/Fe-doped biochar and its dual applications in Cr(VI) removal, *Sep. Purif. Technol.*, 2023, **317**, 123880.

45 X. Weng, M. Guo, F. Luo and Z. Chen, One-step green synthesis of bimetallic Fe/Ni nanoparticles by eucalyptus leaf extract: biomolecules identification, characterization and catalytic activity, *Chem. Eng. J.*, 2017, **308**, 904–911.

46 L. Fang, J.-s. Li, S. Donatello, C. Cheeseman, C. S. Poon and D. C. Tsang, Use of Mg/Ca modified biochars to take up phosphorus from acid-extract of incinerated sewage sludge ash (ISSA) for fertilizer application, *J. Cleaner Prod.*, 2020, **244**, 118853.

47 S. Pandey and S. B. Mishra, Organic–inorganic hybrid of chitosan/organoclay bionanocomposites for hexavalent

chromium uptake, *J. Colloid Interface Sci.*, 2011, **361**, 509–520.

48 R. M. de Souza, H. B. Quesada, L. F. Cusioli, M. R. Fagundes-Klen and R. Bergamasco, Adsorption of non-steroidal anti-inflammatory drug (NSAID) by agro-industrial by-product with chemical and thermal modification: Adsorption studies and mechanism, *Ind. Crops Prod.*, 2021, **161**, 113200.

49 M. Haris, M. Usman, F. Su, W. Lei, A. Saleem, Y. Hamid, J. Guo and Y. Li, Programmable synthesis of exfoliated biochar nanosheets for selective and highly efficient adsorption of thallium, *Chem. Eng. J.*, 2022, **434**, 134842.

50 C. Xiong, W. Wang, F. Tan, F. Luo, J. Chen and X. Qiao, Investigation on the efficiency and mechanism of Cd(II) and Pb(II) removal from aqueous solutions using MgO nanoparticles, *J. Hazard. Mater.*, 2015, **299**, 664–674.

51 S. Chen, C. Qin, T. Wang, F. Chen, X. Li, H. Hou and M. Zhou, Study on the adsorption of dyestuffs with different properties by sludge-rice husk biochar: adsorption capacity, isotherm, kinetic, thermodynamics and mechanism, *J. Hazard. Mater.*, 2019, **285**, 62–74.

52 H. L. Ma, Y. Zhang, Q.-H. Hu, D. Yan, Z. Z. Yu and M. Zhai, Chemical reduction and removal of Cr(VI) from acidic aqueous solution by ethylenediamine-reduced graphene oxide, *J. Mol. Liq.*, 2012, **22**, 5914–5916.

53 Y. Wang, R. Wang, N. Lin, Y. Wang and X. Zhang, Highly efficient microwave-assisted Fenton degradation bisphenol A using iron oxide modified double perovskite intercalated montmorillonite composite nanomaterial as catalyst, *J. Colloid Interface Sci.*, 2021, **594**, 446–459.

54 M. Yu, B. Zhu, J. Yu, X. Wang, C. Zhang and Y. Qin, A biomass carbon prepared from agricultural discarded walnut green peel: investigations into its adsorption characteristics of heavy metal ions in wastewater treatment, *Biomass Convers. Biorefin.*, 2023, **13**, 12833–12847.

55 Y. Wang, Y. Gong, N. Lin, H. Jiang, X. Wei, N. Liu and X. Zhang, Cellulose hydrogel coated nanometer zero-valent iron intercalated montmorillonite (CH-MMT-nFe^0) for enhanced reductive removal of Cr(VI): Characterization, performance, and mechanisms, *J. Mater. Chem.*, 2022, **347**, 118355.